

Trisecting the 9-vertex complex projective plane

Richard Evan Schwartz *

July 5, 2022

Abstract

In this paper we will give a short and direct proof that Wolfgang Kühnel's 9-vertex simplicial complex \mathbf{CP}_9^2 is homeomorphic to \mathbf{CP}^2 , the complex projective plane. The idea of our proof is to recall the trisection of \mathbf{CP}^2 into 3 bi-disks and then to see this trisection inside a symmetry-breaking subdivision of \mathbf{CP}_9^2 . After giving the proof we will elaborate on the construction and sketch an explicit homeomorphism.

1 Introduction

A k -simplex is a k -dimensional convex polytope with $k + 1$ vertices. For $k = 0, 1, 2, 3$ respectively, a k -simplex is usually called a *vertex*, *edge*, *triangle*, *tetrahedron*. When k is not important, a k -simplex is just called a *simplex*.

A *simplicial complex* is a finite collection \mathcal{C} of simplices, all in an ambient Euclidean space, such that

- If $S \in \mathcal{C}$ and S' is a sub-simplex of S then $S' \in \mathcal{C}$.
- If $S, T \in \mathcal{C}$ then $S \cap T$ is either empty or in \mathcal{C} .

Informally, the simplices in a simplicial complex fit together cleanly, without crashing through each other. The *support* $|\mathcal{C}|$ of \mathcal{C} is the union of all the simplices in \mathcal{C} . Often we blur the distinction between \mathcal{C} and $|\mathcal{C}|$ and think of a simplicial complex as a union of simplices.

*Supported by N.S.F. grant D.M.S.-2102803.

A simplicial complex may be described with no mention of the ambient space containing it, but there is always the understanding that in principle one can find an isomorphic complex in some Euclidean space. To give a pertinent example, let \mathbf{RP}_6^2 be the quotient of the regular icosahedron by the antipodal map. This simplicial complex has 6 vertices, 15 edges, and 10 faces. One can reconstruct \mathbf{RP}_6^2 in \mathbf{R}^5 by fixing some 5-simplex $\Sigma \subset \mathbf{R}^5$, the convex hull of vertices v_1, \dots, v_6 , then mapping vertex k of \mathbf{RP}_6^2 to v_k and extending linearly.

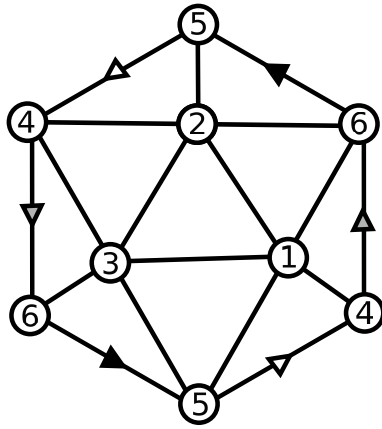


Figure 1: \mathbf{RP}_6^2 , the 6-vertex triangulation of \mathbf{RP}^2 .

Figure 1 shows another incarnation of \mathbf{RP}_6^2 . In this picture, the outer edges of the hexagon are supposed to be identified according to the labels. The complex \mathbf{RP}_6^2 is called a *6-vertex triangulation* of the real projective plane \mathbf{RP}^2 because its support is homeomorphic to \mathbf{RP}^2 . This triangulation has the fewest number of vertices amongst triangulations of \mathbf{RP}^2 , so it is called a *minimal triangulation* of \mathbf{RP}^2 . It is in fact the unique minimal triangulation of \mathbf{RP}^2 . (Smaller examples like the quotient of the regular octahedron by the antipodal map fail to be simplicial complexes.)

Here are some other examples related to minimal triangulations.

- The boundary of a tetrahedron is the unique 4-vertex minimal triangulation of the 2-sphere. More generally, the boundary of a $(k + 1)$ simplex is the unique minimal triangulation of the k -sphere.
- If you identify the opposite sides of the big hexagon in Figure 4 below, you get the unique minimal triangulation T_7^2 of the 2-torus. T_7^2 has 14 triangles, 21 edges, and 7 vertices.

- In 1980, W. Kühnel discovered CP_9^2 , the unique 9-vertex minimal triangulation of the complex projective plane CP^2 . This triangulation has 36 4-simplices and a symmetry group of order 54.
- In 1992, U. Brehm and W. Kühnel [BK] defined HP_{15}^2 (and two variants), a 15-vertex simplicial complex with 490 8-simplices. In 2019, D. Gorodkov [G] proved that HP_{15}^2 and the variants are PL homeomorphic to the quaternionic projective plane HP^2 .
- So far it is an open question as to whether there is a 27-vertex triangulation of OP^2 , the octonionic (a.k.a. Cayley) projective plane.
- The minimal triangulations of RP^3 and RP^4 respectively have 11 and 16 vertices. See [D],
- In 2021, K. Adiprasito, S. Avvakumov, R. Karasev [AAK] proved that real projective space can be triangulated using a sub-exponential number of simplices.

The survey article by B. Datta [D] has a wealth of information about minimal triangulations up to the year 2007 and a large number of references.

The subject of this paper is CP_9^2 . In [KB], Kühnel and T. Banchoff establish many interesting properties of CP_9^2 and give a rather intricate proof that CP_9^2 really is homeomorphic to CP^2 . Since [KB], there has been a lot of work done trying to understand CP_9^2 from various points of view. In particular, there are a number of proofs that $CP_9^2 \cong CP^2$, and also a number of proofs that CP_9^2 is the only minimal triangulation of CP^2 . See the article by B. Morin and M. Yoshida [MY] for a survey of these proofs. See also the paper by B. Bagchi and B. Datta [BD].

The purpose of this paper is to give a new and very nice proof that $CP_9^2 \cong CP^2$. The basic idea of the proof here is to recall the trisection of CP^2 into 3 bi-disks, and then to see this trisection inside a symmetry-breaking subdivision of CP_9^2 . The construction is perfectly compatible with an easier version that works for RP_6^2 , so I will explain that as well.

The picture developed here is related to the 10-vertex triangulation CP_{10}^2 of CP^2 that in [BK] is constructed by building outward from T_7^2 . Indeed Denis Gorodkov, in a private communication, explained to me how one can find a “path” from CP_9^2 to CP_{10}^2 using the subdivision idea and then something akin to bi-stellar flips. (I’ll let Denis tell this story elsewhere if he wants to, but see the end of §2 for a hint.)

My proof also has a close kinship with the “red-white-blue discussion” in §1.3 of the M.P.I.M. preprint by Morin and Yoshida that is the precursor to [MY] (and has the same title). This discussion is, in turn, related to Figure 8 in [KB]. Morin and Yoshida describe the red-white-blue discussion as a “topological insight” but they don’t really push it forward into a proof. I think that my picture is very similar, but clarified by the special subdivision.

The approach here possibly could shed light on Gorodkov’s result that $\mathbf{HP}_{15}^2 \cong \mathbf{HP}^2$. The same subdivision and trisection ideas go through for \mathbf{HP}_{15}^2 almost *verbatim*, and I can see computationally that each of the 3 sub-complexes is shellable and therefore PL homeomorphic to an 8-ball. However, the high dimensional topology involved in analyzing \mathbf{HP}_{15}^2 makes a direct topological analysis of the whole complex formidable. For instance, the sub-complex that plays the role of T_7^2 has 288 6-simplices. A key step in extending the proof here to \mathbf{HP}_{15}^2 would be showing that this 288-monster is homeomorphic to $(S^3 \times S^3 \times S^3)/S^3$ in a 3-fold symmetric way.

Here is an outline of the paper.

- In §2 I will give the analogous version of my proof for \mathbf{RP}_6^2 . This case is quite concrete and one can see the whole idea at a glance.
- In §3 I will recall the trisection of \mathbf{CP}^2 and discuss a few key properties of the *central torus* in this decomposition.
- In §4 I will describe \mathbf{CP}_9^2 and then explain my symmetry-breaking subdivision. The construction parallels the real case.
- In §5 I will find the trisection inside the subdivision and construct a homeomorphism $h : \mathbf{CP}_9^2 \rightarrow \mathbf{CP}^2$ which respects the trisections.
- In §6 I will explain how one can see the real case of the construction inside the complex case. This analysis leads to a refinement of h and gives the full power of our main result, Theorem 5.1.
- In §7 I will sketch how to make h completely explicit.

I thank Tom Banchoff, Kenny Blakey, Thomas Goodwillie, Denis Gorodkov, Joe Hlavinka, Wolfgang Kühnel, Tyler Lane, Dennis Sullivan, and Oleg Viro for helpful discussions. (Many of these discussions were about issues related to \mathbf{HP}_{15}^2 .) I also thank the anonymous referee for a number of helpful comments, especially those pertaining to the real case of the construction. These comments from the referee inspired §6-7.

2 The Real Case

\mathbf{RP}^2 is the space of scale equivalence classes of nonzero vectors in \mathbf{R}^3 . We denote the equivalence class of $(x_1, x_2, x_3) \in \mathbf{R}^3$ by $[x_1 : x_2 : x_3] \in \mathbf{RP}^2$.

We have the *trisection* $\mathbf{RP}^2 = \beta_1 \cup \beta_2 \cup \beta_3$, where β_j is the set where $\max(|x_1|, |x_2|, |x_3|) = |x_j|$. Points in β_1 may be written uniquely in the form $[1 : x_2 : x_3]$, with $|x_2|, |x_3| \leq 1$. Thus β_1 is a square. So are β_2 and β_3 . Each intersection $\beta_i \cap \beta_j$ is a pair of opposite edges, and the triple intersection is a union of the 4 points $[\pm 1 : \pm 1 : \pm 1]$. If we interpret \mathbf{RP}^2 as the quotient of a cube by the antipodal map, then the 3 quotient faces are $\beta_1, \beta_2, \beta_3$.

The trisection has 3-fold symmetry. The map $\Sigma : (x_1, x_2, x_3) \rightarrow (x_2, x_3, x_1)$ permutes the sets $\beta_1, \beta_2, \beta_3$. In terms of the cube, Σ rotates around the appropriate long diagonal. \mathbf{RP}_6^2 has a very similar 3-fold symmetry: The permutation $S = (123)(456)$ acts as a rotational symmetry of \mathbf{RP}_6^2 .

We add a new vertex $[123]$ at the center of the triangle $(1, 2, 3)$, and also new vertices $[12], [13], [23]$ at the centers of the corresponding edges.

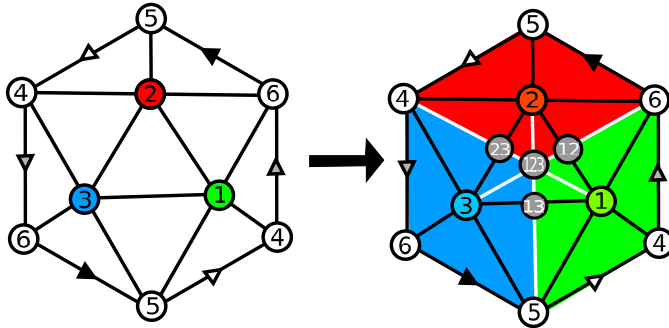


Figure 2: A subdivision of \mathbf{RP}_6^2 into 18 triangles.

Using the new vertices, we divide the central triangle of \mathbf{RP}_6^2 into 6 triangles and we subdivide each of the adjacent triangles in half. The subdivision has $18 = 3 \times 6$ triangles, with each having exactly one vertex from the set $\{1, 2, 3\}$. For $j = 1, 2, 3$ we let B_k be the subset of 6 new triangles having k for a vertex. The sets B_1, B_2, B_3 are colored green, red, blue in Figure 2.

This is now the trisection, and there is a clear homeomorphism from this subdivided complex to \mathbf{RP}^2 which maps B_j to β_j and conjugates S to Σ .

Incidentally, a related approach would be to add only $[123]$ and then to replace the sides $(1, 2)$, $(2, 3)$, $(3, 1)$ with the sides $([123], 6)$, $([123], 5)$ and $([123], 4)$. Gorodkov's "path" from \mathbf{CP}_9^2 to \mathbf{CP}_2^{10} is a more elaborate complex-number analogue of this.

3 The Smooth Trisection: Complex Case

The complex projective plane \mathbf{CP}^2 is defined just as \mathbf{RP}^2 but with respect to the field \mathbf{C} of complex numbers. We denote points in \mathbf{CP}^2 by $[z_1 : z_4 : z_7]$. The variable names will line up with the notation for \mathbf{CP}_9^2 . We have the trisection $\mathbf{CP}^2 = \beta_1 \cup \beta_4 \cup \beta_7$, where β_j is defined just as in the real case, using the complex norm in place of the absolute value. This time, β_j is the product of 2 unit disks. The bi-disks $\beta_1, \beta_4, \beta_7$ have disjoint interiors and are permuted by the same map Σ as defined in the real case.

The boundary $\partial\beta_1$ is a 3-sphere, and it decomposes into the solid tori β_{14} and β_{17} . Here $\beta_{ij} = \beta_i \cap \beta_j$. To see that β_{14} is a solid torus, note that β_{14} consists of points of the form $[1 : u : z]$ with $|z| \leq |u| = 1$ and is therefore the product of the unit disk and the unit circle. The *central torus* $\beta_{147} = \beta_{14} \cap \beta_{17} = \beta_1 \cap \beta_4 \cap \beta_7$ consists of points where $|z_1| = |z_4| = |z_7|$. We discuss β_{147} in more detail, with a view towards seeing it inside \mathbf{CP}_9^2 .

Hexagonal Structure: Let $\mathbf{R}_0^3 \subset \mathbf{R}^3$ denote the plane of points whose coordinates sum to 0. Let $H = \mathbf{R}_0^3 \cap [-1, 1]^3$. The vertices of this regular hexagon are the permutations of $(1, -1, 0)$. Let \overline{H} be the flat torus obtained by identifying the opposite sides of H by translations. The translation vectors are the cyclic permutations of $\pm(1, 1, -2)$. The map

$$(x_1, x_4, x_7) \rightarrow [x_1^* : x_4^* : x_7^*], \quad x^* = e^{\frac{2\pi i x}{3}}$$

induces a homeomorphism $\overline{H} \rightarrow \beta_{147}$. The main point behind this fact is that $[1^* : 1^* : (-2)^*] = [0^* : 0^* : 0^*]$, etc. We equip β_{147} with the metric which makes $\overline{H} \rightarrow \beta_{147}$ an isometry.

Symmetries: The 3 fixed points of Σ lie in β_{147} and correspond to the points on \overline{H} represented by the center and vertices of H . The fixed point set of coordinatewise complex conjugation, which we call \mathcal{T} , is \mathbf{RP}^2 . Note that $\mathbf{RP}^2 \cap \beta_{147} = \{[\pm 1 : \pm 1 : \pm 1]\}$. These points correspond to the center of H and to the centers of the edges of H .

A Contractible Loop: The line in \mathbf{R}_0^3 where $x_1 = x_4$ bisects H and contains the midpoints of a pair of opposite sides. This line gives rise to a geodesic loop in \overline{H} . See the loop a_{14} in Figure 4 below. The corresponding loop $\alpha_{14} \subset \beta_{147}$ is given by $\{[1 : 1 : u] \mid |u| = 1\}$. The loop α_{14} is contractible in β_{14} : It bounds the disk in β_{14} consisting of points $[1 : 1 : z]$ with $|z| \leq 1$.

4 The Complex and its Subdivision

The vertices of \mathbf{CP}_9^2 are labeled $1, \dots, 9$. Here are 16 of the 36 4-simplices of \mathbf{CP}_9^2 listed on p. 15 of [KB].

- 15289 12389 13689 45289 42389 43689
- 14256 14356 14259 14368
- 14726 14768 (14783 14735 14759 14792)

Comparing our list to [KB], we have sometimes permuted the vertices so as to highlight the indices $1, 4, 7$. The other 24 4-simplices are orbits of the first 12 under the action of the *fundamental permutation*:

$$S = (147)(258)(369).$$

For instance, 14726 has orbit $14726 \rightarrow 14759 \rightarrow 14783$. The four simplices in parentheses are listed for the sake of making our tetrahedron list below more transparent. In [KB] the authors exhibit a symmetry group of order 54 acting on \mathbf{CP}_9^2 . For us, one other special element of this group is the symmetry $T = (23)(56)(89)$.

Let $[ij]$ be the midpoint of the edge $i \leftrightarrow j$. Let $[ijk]$ be the center of the triangle ijk . Let the *rank* of a simplex be the number of vertices which belong to the set $\{1, 4, 7\}$. Our list above goes by rank. Parallel to the real case, we divide each rank k simplex into $k!$ smaller simplices, as follows: The rank 1 simplices are untouched. The rank 2 simplex $14abc$ divides into

$$1[14]abc \quad 4[14]abc,$$

and likewise with the indices $1, 4, 7$ permuted. The rank 3 simplex $147ab$ divides into

$$1[14][147]ab \quad 1[17][147]ab \quad 4[14][147]ab \quad 4[47][147]ab \quad 7[17][147]ab \quad 7[47][147]ab.$$

We replace our original 36 simplices with the subdivided simplices. Since there are respectively 18, 12, 6 simplices of rank 1, 2, 3 we get a total of

$$(1, 2, 6) \cdot (18, 12, 6) = 78 = 3 \times 26$$

new simplices. (The rank 1 simplices count as “new”.) Each new simplex has exactly one vertex from the set $\{1, 4, 7\}$.

5 The Combinatorial Trisection

We have $\mathbf{CP}_9^2 = B_1 \cup B_4 \cup B_7$, where B_j is the union of the 26 new simplices having $j \in \{1, 4, 7\}$ as a vertex. Each B_j is the cone to vertex j of ∂B_j . Hence B_i and B_j have disjoint interiors for $i \neq j$. Here is our main result.

Theorem 5.1 *There is a homeomorphism $h : \mathbf{CP}_9^2 \rightarrow \mathbf{CP}^2$ with the following properties:*

1. h maps vertices 1, 4, 7 respectively to $[1 : 0 : 0]$, $[0 : 1 : 0]$, $[0 : 0 : 1]$.
2. h maps B_j to β_j for $j = 1, 4, 7$.
3. h conjugates S to Σ .
4. h conjugates T to \mathcal{T} .

In this section I will construct a non-explicit homeomorphism h which has the first 3 properties but not necessarily the fourth. This should satisfy a reader who just wants to see why $\mathbf{CP}_9^2 \cong \mathbf{CP}^2$. In §6, I will give a more refined version of h which has the fourth property. In §7 I will sketch how to make h explicit.

The first thing we do is list the tetrahedra in $B_{14} = B_1 \cap B_4$. We will derive this tetrahedron list from the simplex list above. The reader might want to check that this actually works, so for convenience we repeat the simplex list here:

- 15289 12389 13689 45289 42389 43689
- 14256 14356 14259 14368
- 14726 14768 (14783 14735 14759 14792)

Now for the derivation. We get 13 tetrahedra contained in B_{14} by subdividing the simplices on our list above and omitting 1 or 4. The tetrahedra are listed in a way that corresponds to the simplices.

- 5289 2389 3689
- [14]256 [14]356 [14]259 [14]368
- [14][147]26 [14][147]68 [14][147]83 [14][147]35 [14][147]59 [14][147]92

The images of these 13 tetrahedra under S^{-1} lie in B_{17} and are totally distinct from the ones above. This accounts for all 26 tetrahedra in ∂B_1 . Hence, the 13 above are the complete list of tetrahedra comprising B_{14} , and moreover B_{14} and B_{17} have disjoint interiors.

Lemma 5.2 B_{14} is a solid torus.

Proof: Write $B_{14} = B'_{14} \cup B''_{14}$, where B'_{14} is the union of the first 3 tetrahedra above and B''_{14} is the union of the last ten. B'_{14} is a 3-ball because it is the join of the path 5236 with the segment 89, and B''_{14} is a 3-ball because it is the cone to vertex [14] of $\partial B''_{14}$, a 10-triangle triangulation of the 2-sphere.

Figure 3 below shows $\partial B'_{14}$ and $\partial B''_{14}$. Each one is drawn as the union of 2 combinatorial hexagons glued along their boundaries according to the labels. $B'_{14} \cap B''_{14}$ is the union of the 2 disjoint grey triangles 259 and 368. Topologically, we get B_{14} by gluing two 3-balls together along a pair of disjoint disks in their boundaries. The orientations of the gluings are such that the result is a solid torus (as opposed to the so-called solid Klein bottle, a nontrivial disk bundle over the circle). ♠

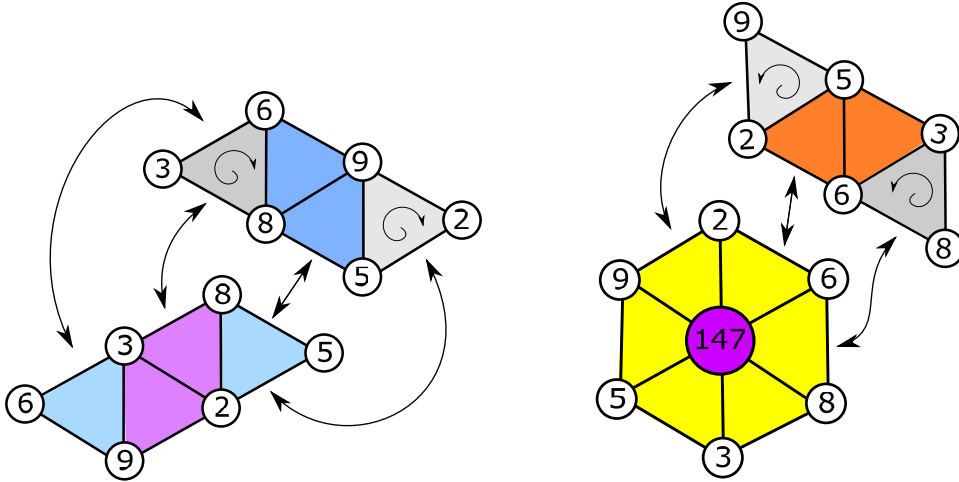


Figure 3: $\partial B'_{14}$ and $\partial B''_{14}$. Glue the hex boundaries together.

We get the triangulation of $B_{147} = \partial B_{14}$ by gluing the two triangulations from Figure 3 along the grey triangles. Figure 4 shows the universal cover of the triangulation. We get back to B_{147} by gluing the opposite sides of the big hexagon by translations. This triangulation of B_{147} is exactly T_7^2 . Note that

S acts on B_{147} fixing $[147]$, $[258]$, $[369]$, points which respectively correspond to the center and vertices of the hexagon, just as in the smooth case.

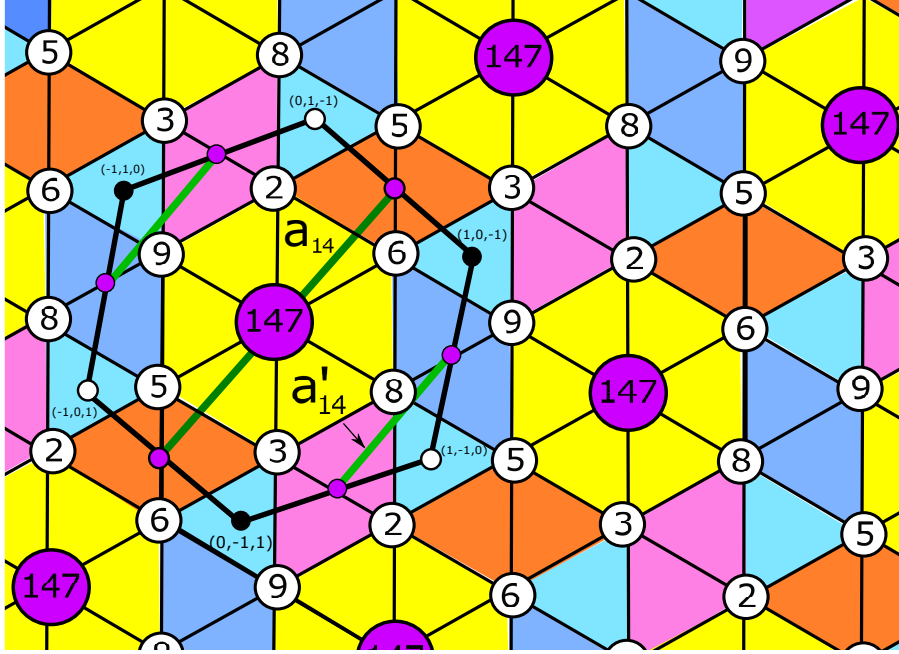


Figure 4: The universal covering of the triangulation of B_{147} .

From all this structure we see that (after suitably scaling) there is an isometry $h_{147} : B_{147} \rightarrow \beta_{147}$ which conjugates S to Σ and which maps the green loop a_{14} to α_{14} . The labels of the hexagon vertices, such as $(1, -1, 0)$, indicate precisely how the hexagon here lines up with the one described in connection with the central torus of \mathbf{CP}^2 . Note that a_{14} is contractible in B_{14} because $a_{14} \subset B''_{14}$, and recall that α_{14} is contractible in β_{14} . Hence h_{147} extends to a homeomorphism $h_{14} : B_{14} \rightarrow \beta_{14}$.

Define $h_{17} = \Sigma^{-1} \circ h_{14} \circ S$ and $h_{47} = \Sigma \circ h_{14} \circ S^{-1}$. This gives us homeomorphisms $h_{17} : B_{17} \rightarrow \beta_{17}$ and $h_{47} : B_{47} \rightarrow \beta_{47}$. The maps h_{ij} all agree on B_{147} because h_{147} conjugates S to Σ . The union

$$h = h_{14} \cup h_{17} \cup h_{47} : \partial B_1 \cup \partial B_4 \cup \partial B_7 \rightarrow \partial \beta_1 \cup \partial \beta_4 \cup \partial \beta_7$$

is a homeomorphism which respects the individual pieces and their intersections. Since B_j and β_j are cones over ∂B_j and $\partial \beta_j$ we can extend h , by coning, to a homeomorphism from $\mathbf{CP}_9^2 = B_1 \cup B_4 \cup B_7$ to $\mathbf{CP}^2 = \beta_1 \cup \beta_4 \cup \beta_7$.

6 The Extra Symmetry

The fixed set of $T = (23)(56)(89)$ is a copy of \mathbf{RP}_6^2 . The 6 vertices are 1, 4, 7, [23], [89], [56]. If we rename these vertices $\hat{1}, \hat{2}, \hat{3}, \hat{4}, \hat{5}, \hat{6}$ we get the same combinatorial pattern as in Figure 1. Our subdivision of \mathbf{CP}_9^2 induces the same subdivision as in Figure 2. In particular, the intersection $\mathbf{RP}_6^2 \cap B_{14}$ is a union of 3 edges which together make 2 line segments, namely

$$\hat{4}\hat{5} = [23][89] \subset B'_{14}, \quad \hat{6}[\hat{1}\hat{2}], [\hat{1}\hat{2}][\hat{1}\hat{2}\hat{3}] = [56][14], [14][147] \subset B''_{14}.$$

The map h_{147} conjugates T to \mathcal{T} . Figure 5 below indicates how h_{147} maps the fixed points of T in B_{147} to the fixed points of \mathcal{T} in β_{147} .

Now we explain how to choose our homeomorphism h so that it conjugates T to \mathcal{T} . Figure 5 below illustrates the following 4 disks.

- Let D'_{14} be the cone to $[[23][89]]$ of the loop a'_{14} shown in Figure 4.
- Let D''_{14} be the cone to [14] of the loop a_{14} shown in Figure 4.
- Let Δ'_{14} be the disk $[1 : -1 : z]$ with $|z| \leq 1$. We think of Δ'_{14} as the cone to $[1 : -1 : 0]$ of $\partial\Delta'_{14}$.
- Let Δ''_{14} be the disk $[1 : 1 : z]$ with $|z| \leq 1$. We think of Δ''_{14} as the cone to $[1 : 1 : 0]$ of $\partial\Delta''_{14}$.

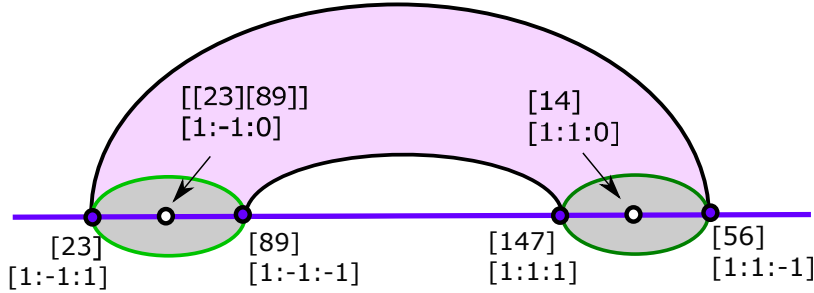


Figure 5: One component of X_{14} or of χ_{14} , depending on the label choice.

Let Y_{14} be the component of $B_{14} - D'_{14} - D''_{14}$ that contains the point [259]. Let Υ_{14} be the component of $\beta_{14} - \Delta'_{14} - \Delta''_{14}$ which contains the point $[1 : 1 : i]$. Both Y_{14} and Υ_{14} are solid balls. T interchanges Y_{14} with (the closure of) $B_{14} - Y_{14}$, the other component of $B_{14} - D'_{14} - D''_{14}$. Likewise \mathcal{T} interchanges Υ_{14} with (the closure of) $\beta_{14} - \Upsilon_{14}$.

When we use the top label of each pair, Figure 5 shows Y_{14} . (Think about cutting a pink-frosted grey donut in half.) The pink boundary is half of B_{147} . The left grey disk is D'_{14} and the right grey disk is D''_{14} . The map T acts as rotation by 180 degrees about the purple line bisecting the grey disks. The intersection of the purple line with the grey disks is the part lying in our copy of \mathbf{RP}_6^2 . When we use the bottom labels, Figure 5 shows the same things for Υ_{14} .

By construction $h_{147}(\partial D'_{14}) = \partial \Delta'_{14}$ and $h_{147}(\partial D''_{14}) = \partial \Delta''_{14}$. We define h_{14} on each of D'_{14} and D''_{14} by coning over the boundaries. By symmetry this extension conjugates T to \mathcal{T} and is defined in particular on ∂Y_{14} . Our extension maps the (pink and grey) sphere ∂Y_{14} to the (pink and grey) sphere $\partial \Upsilon_{14}$. We now extend to a homeomorphism from the ball Y_{14} to the ball Υ_{14} and use the action of T and \mathcal{T} to extend the homeomorphism to all of B_{14} . Our improved h_{14} conjugates T to \mathcal{T} .

The rest of the construction is as above. The union map $h_{14} \cup h_{17} \cup h_{47}$, defined on $\partial B_1 \cup \partial B_4 \cup \partial B_7$, conjugates T to \mathcal{T} because the pairs (S, T) and (Σ, \mathcal{T}) commute. The final coning process respects T and \mathcal{T} , so the final extension of h to $B_1 \cup B_4 \cup B_7$ conjugates T to \mathcal{T} .

Here is where h sends the vertices:

- $1 \rightarrow [1 : 0 : 0]$.
- $[14] \rightarrow [1 : 1 : 0]$.
- $[147] \rightarrow [1 : 1 : 1]$.
- $[56] \rightarrow [1 : 1 : -1]$.
- $2 \rightarrow [1 : e^{4\pi i/7} : e^{12\pi i/7}]$.
- $[259] \rightarrow [1 : e^{4\pi i/7} : 0]$.

The remaining images can be readily deduced from the action of $S, T, \Sigma, \mathcal{T}$. The last two entries require some explanation. The coordinates of the point $p_2 \in \mathbf{R}_0^2$ corresponding to vertex 2 are $(-1, 5, -4)/7$. We found this by solving the equation $2p_2 - \Sigma^2(p_2) = (-1, 2, -1)$. The choice of where to send $[259]$ is not determined by the construction above, but we might as well make it. The explicit construction below makes this choice, and so it is convenient to list it here.

7 Making the Homeomorphism Explicit

The only non-explicit part of our construction is the extension of the sphere map $h_{147} : \partial Y_{14} \rightarrow \partial \Upsilon_{14}$ to the ball map $h_{14} : Y_{14} \rightarrow \Upsilon_{14}$. In this section we sketch an explicit extension.

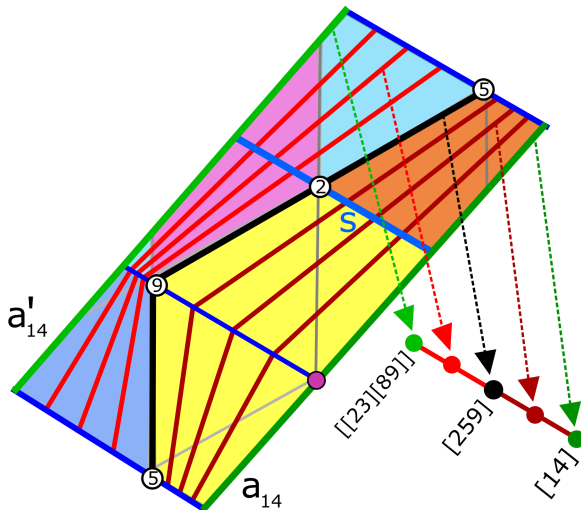


Figure 6: A foliation of $\partial Y_{14} - D'_{14} - D''_{14}$, and the core of Y_{14} .

Gluing the opposite blue sides of the parallelogram in Figure 6 gives the cylinder $\partial Y_{14} - D'_{14} - D''_{14}$, drawn pink in Figure 5. The green loops a_{14} and $a_{14'}$ are on the boundary. Figure 6 suggests an explicit foliation of ∂Y_{14} by polygonal loops. Intrinsically these are geodesic bigons in B_{147} . The intersections with the blue edges of the triangulation move linearly.

Let the *core* of Y_{14} be the path with vertices $[14]$, $[259]$, $[[23][89]]$. Figure 6 indicates a piecewise linear correspondence between the loops in the foliation and the points on the core. We cone each loop in the foliation to the corresponding point on the core. Now (after some checking of disjointness) we have a disk foliation of Y_{14} which interpolates between D'_{14} and D''_{14} and respects the partition of Y_{14} into $Y_{14} \cap B'_{14}$ and $Y_{14} \cap B''_{14}$.

We use h_{147} to transfer our foliation to $\partial \Upsilon_{14} - \Delta'_{14} - \Delta''_{14}$. We change coordinates:

$$[1 : u : z] \rightarrow (\arg u, z).$$

In these coordinates, $\Upsilon_{14} = [0, \pi] \times D^2$. Let s be the blue line segment in Figure 6 that runs all the way across the cylinder and contains vertex 2. The

intersection $(t_\gamma, z_\gamma) = \gamma \cap s$ is a center of symmetry of the loop γ . We cone γ to $(t_\gamma, 0)$. Now (after some checking of disjointness) we have a disk foliation of Υ_{14} which interpolates between Δ'_{14} and Δ''_{14} .

We extend h_{147} to Y_{14} by coning, so that it maps the one foliation to the other. This description explicitly determines $h_{14} : Y_{14} \rightarrow \Upsilon_{14}$. Again, the rest of the construction is just symmetry and coning, so that final map h is explicitly defined.

8 References

- [AAK], K. Adiprasito, S. Avvakumov, R. Karasev, *A subexponential size triangulation of \mathbf{RP}^n* , *Combinatorica* **42**, 1-8 (2022)
- [BD] B. Bagchi and B. Datta, *A short proof of the uniqueness of Kühnel's 9-vertex complex projective plane*, *Advances in Geometry* (2001) pp 157-163.
- [BK] T. Banchoff and W Kühnel, *Equilibrium triangulations of the complex projective plane*, *Geometriae Dedicata* **44** (1992) pp 311-333
- [BrK] U. Brehm and W Kühnel, *15-vertex triangulations of an 8-manifold*, *Math Annalen* **294** (1992) pp 167–193
- [D] B. Datta, *Minimal Triangulations of Manifolds*, *Journal of the Indian Institute of Science*, Vol. 87, No. 4, (2007) pp. 429-450.
(See also arXiv:math/0701735v1)
- [G] D. Gorodkov, *A 15-Vertex Triangulation of the Quaternionic Projective Plane*, *Discrete Computational Geometry*, (Sept 2019) pp 348-373
- [KB]: W. Kühnel and T. F. Banchoff, *The 9-Vertex Complex Projective Plane*, *Math. Intelligencer*. Vol 5, No 3 (1983) pp 11-22
- [MY] B. Morin and M. Yoshida, *The Kühnel triangulation of the complex projective plane from the point of view of complex crystallography*, *Mem. Fac. Sci. Kyushu Univ. Ser. A* **45** (1991) pp 55-142